



## COUPLED BISTABLE MAPS: A TOOL TO STUDY CONVECTION PARAMETERIZATION IN OCEAN MODELS

PEDRO G. LIND<sup>\*,†,‡</sup>, SVEN TITZ<sup>§</sup>, TILL KUHLBRODT<sup>||</sup>,  
JOÃO A. M. CORTE-REAL<sup>\*,†,††</sup>, JÜRGEN KURTHS<sup>§</sup>,  
JASON A. C. GALLAS<sup>\*,†,‡,¶</sup> and ULRIKE FEUDEL<sup>\*\*</sup>

*\*Centro de Geofísica, Universidade de Évora,  
7000 Évora, Portugal*

*†Instituto de Física, Universidade Federal do Rio Grande do Sul,  
91501-970 Porto Alegre, Brazil*

*‡Unidade de Meteorologia e Climatologia,  
Instituto de Ciência Aplicada e Tecnologia,  
Faculdade de Ciências, Universidade de Lisboa,  
1749-016 Lisboa, Portugal*

*§Arbeitsgruppe Nichtlineare Dynamik, Institut für Physik,  
Universität Potsdam, D-14415 Potsdam, Germany*

*||Potsdam-Institut für Klimafolgenforschung,  
D-14412 Potsdam, Germany*

*¶Institut für Computeranwendungen, Universität Stuttgart,  
Pfaffenwaldring 27, D-70569 Stuttgart, Germany*

*\*\*Institut für Chemie und Biologie des Meeres,  
Universität Oldenburg, D-26111 Oldenburg, Germany*

*††jcr@fc.ul.pt*

Received February 3, 2003; Revised March 12, 2003

We present a study of ocean convection parameterization based on a novel approach which includes both eddy diffusion and advection and consists of a two-dimensional lattice of bistable maps. This approach retains important features of usual grid models and allows to assess the relative roles of diffusion and advection in the spreading of convective cells. For large diffusion our model exhibits a phase transition from convective patterns to a homogeneous state over the entire lattice. In hysteresis experiments we find staircase behavior depending on stability thresholds of local convection patterns. This nonphysical behavior is suspected to induce spurious abrupt changes in the spreading of convection in ocean models. The final steady state of convective cells depends not only on the magnitude of the advective velocity but also on its direction, implying a possible bias in the development of convective patterns. Such bias points to the need for an appropriate choice of grid geometry in ocean modeling.

*Keywords:* Oceanic convection; ocean modeling; model grid; coupled map lattice; bistable maps.

## 1. Introduction

An important and difficult problem in geophysical fluid dynamics is to develop efficient and reliable computer codes for modeling numerically complex spatiotemporal phenomena. For example, the numerical modeling of ocean dynamics is based on a discretization of the partial differential equations which describe how the fields of velocity, temperature, pressure and salt content evolve [Peixoto & Oort, 1992; Heidvogel & Beckmann, 1998]. Depending on the space and time scales used, this discretization yields a hierarchy of models. They go from the relatively simple “box models” [Rahmstorf, 2001], based on a small number of subsystems, up to large grid models, when a rigid time-step and mostly a rectangular grid are used and subgrid processes are parameterized [Heidvogel & Beckmann, 1998; Haltiner & Williams, 1992]. The latter models lead to reasonable results but a few physical processes are not very well represented, especially when they involve a subgrid scale and are highly nonlinear. One such nonlinear process is convection. Despite being a small scale process, convection competes with the large scale process of eddy diffusion and advection in determining ocean circulation. Since convection is a subgrid-scale and a nonhydrostatic process, it needs to be parameterized.

The common parameterization of convection (as applied to 3D ocean models) is called convective adjustment (CA) and works as follows: whenever the water density at a grid point in any layer becomes larger than the water density in the underlying grid point, the water volumes of the two grid boxes are instantaneously mixed, i.e. the two grid points are set to the same averaged temperature and salinity. Now, this convective adjustment scheme induces an extremely strong nonlinearity into the system which can be studied with simple box models [Welander, 1982; Lenderink & Haarsma, 1994]. In convection box models, the CA scheme is applied to two vertically adjacent grid boxes in contact with the environment [Lenderink & Haarsma, 1994]. Using convection box models it can be shown that, for certain conditions, the local convection dynamics is bistable: both permanent convection and permanent density stratification (no convection) are then coexisting stable stationary states of the system. This local bistability in a discretized model grid suggests the introduction of an approach based on coupled map lattices [Kaneko, 1993; Kaneko & Tsuda, 2000].

The aim of the present paper is to introduce a novel approach, based on coupled map lattices, to study convection parameterization. Coupled map lattices (CMLs) consist of a coupled grid of discrete sites in which every site has its (local) dynamics governed by a given map (function). Both time and space are discretized in CMLs. For a suitable bistable cubic map [Cabral *et al.*, 1993; Brunnet & Gallas, 1998; Kapral & Oppo, 1986], this paper shows how CMLs can be used as an idealization of the convection parameterization in ocean circulation models. While purely diffusive CMLs work well, a much more realistic modeling is obtained when advection is also incorporated [Lind *et al.*, 2002a, 2002b].

CMLs are currently widely used as models for studying pattern formation and spatiotemporal chaos, having many applications in several fields such as optics, quantum field theory [Beck, 1995; Hilgers & Beck, 2001], KPZ equations [Pikovsky & Kurths, 1994], biophysics, fluid dynamics, chemical reactions, plasma physics, etc. [Kaneko, 1993; Kaneko & Tsuda, 2000]. Pattern formation occurs in ocean models as well. Some authors found multiple equilibria of convection *patterns* in ocean models with CA [Lenderink & Haarsma, 1994; Rahmstorf, 1995; Vellinga, 1998]. The existence of different equilibria has been shown to be a consequence of local convective bistability. It is still a matter of debate whether these multiple equilibria are physical or rather artifacts of the CA scheme. In a study with a high-resolution 3D-model it was recently shown [Molemaker & Dijkstra, 2000] that the commonly used CA scheme can introduce erroneous grid scale variability. A similar behavior was found in [Cessi, 1996] where a simplified model for CA exhibits grid-scale instability. The interaction of CA with horizontal diffusion was studied with a one-dimensional CML in [Cessi & Young, 1996] where sensitivity to small changes in the initial conditions was detected.

Whereas the latter two studies were performed with local oscillating dynamics in a one-dimensional CML, the present work uses a two-dimensional CML with local bistable dynamics. The reason for that lies on the assumption that, as is known [Lenderink & Haarsma, 1994; Kuhlbrodt *et al.*, 2001], different areas of the North Atlantic may operate in three different regimes: (i) monostable and nonconvective, (ii) monostable and convective or (iii) *bistable*. Thus, the existence of these three regimes indicates that a reasonable way of

mimicking this dynamics could be to use a CML ruled by a local map supporting two stable attractors capable of coexisting over some domain. Furthermore, in a study of tracer advection schemes it was shown [Hecht *et al.*, 2000] that some advection schemes behave in a very different way after tilting the horizontal grid by  $45^\circ$ . From these studies of the CA algorithm and of advection schemes it can be concluded that modeling convection with CA exhibits complex behavior that is not yet fully understood, and this motivates the present study.

In this paper we investigate the development of convective patterns in ocean models with CA scheme both with and without advection, using a two-dimensional CML model. As will be seen, with the CML model it is not difficult to isolate the main physical processes, such as diffusion and advection, in order to detect and investigate those effects and artifacts of the CA scheme that may be hidden or hard to identify when the full physics is modeled. The present study extends a previous investigation of the effects of advection on a one-dimensional ring of maps [Lind *et al.*, 2002a, 2002b] by investigating the role of advection in a horizontally extended (two-dimensional) CML.

The heart of the two-dimensional CML that we introduce to model ocean convection consists of a local cubic map  $f(x_t) \equiv f(x_t(i, j))$  defined at each site  $(i, j)$  of the lattice by

$$x_{t+1} = f(x_t) = -x_t^3 + ax_t + b, \quad (1)$$

where  $a$  and  $b$  are local control parameters [Cabral *et al.*, 1993; Brunnet & Gallas, 1998; Kapral & Oppo, 1986]. In this map,  $b$  controls the bistability and plays the same role as surface fluxes of heat and freshwater in a convection box model. The amplitudes  $x_t$  represent the stratification of the ocean. If  $x_t$  is positive, there is no or weak stratification, whereas negative  $x_t$  indicates strong stratification. The maps are coupled by eddy diffusion and advection. Thus, we have a two-dimensional CML representing three fundamental processes, each one controlled by a physical quantity: convective bistability by parameter  $b$ , eddy diffusion by the diffusion constant, and advection by the velocity vector. With this tool, we investigate the relative roles of diffusion and advection in the spreading and transport of convective patterns.

The paper is organized as follows: Section 2 describes the diffusive CML model for ocean convection, presenting general results concerning boundary conditions, initial conditions, and bistable local

dynamics. Then we present results obtained using purely diffusive models. First, in Sec. 3, we consider the general behavior of convective and nonconvective states for two sets of initial conditions of great interest. After that, in Sec. 4, we present the distributions of the convective and nonconvective states which characterize the bistable regime in ocean circulation. Furthermore, since some parameters depend on the latitude in the climate system, we consider both homogeneous and heterogeneous parameter distributions in the local cubic map. In addition, Sec. 4 reports some hysteresis experiments showing that local patterns can sensitively determine the global behavior when certain thresholds of the bistability parameter  $b$  are overcome. Next, in Sec. 5, in addition to diffusion, we investigate the effect of advection as recently introduced in CML models [Lind *et al.*, 2002a]. When including advection we find that the final steady states attained by convective patterns depend strongly not only on the magnitude of the velocity vector but also on its direction. Finally, Sec. 6 presents our conclusions and discusses the relevance of these results for 3D ocean models.

## 2. The Diffusive CML Model of Ocean Convection

As is well known [Kaneko, 1993; Kaneko & Tsuda, 2000; Lind *et al.*, 2001a], the time evolution on a purely diffusive lattice of coupled maps is governed by

$$x_{t+1}(i, j) = f(x_t(i, j)) + \varepsilon \mathcal{D}_{i,j}(t), \quad (2)$$

where  $f(x_t(i, j))$  represents the local map (defined by Eq. (1) in the present paper), and  $\mathcal{D}_{i,j}(t)$  represents a two-dimensional discretization of the diffusion operator,

$$\begin{aligned} \mathcal{D}_{i,j}(t) = \frac{1}{4} [ & f(x_t(i+1, j)) + f(x_t(i-1, j)) \\ & + f(x_t(i, j+1)) + f(x_t(i, j-1)) \\ & - 4f(x_t(i, j)) ], \end{aligned} \quad (3)$$

where  $\varepsilon$  ( $0 \leq \varepsilon \leq 1$ ) is the coupling strength, regarded here as the eddy diffusion constant in the ocean,  $i$  and  $j$  label individual sites and take integer values between 1 and  $L$ , inclusive. As already mentioned, the function  $f(x)$  represents the nonlinear map which rules the local dynamics in each site  $(i, j)$  of the lattice.

In ocean models, the diffusion is computed from  $x_t(i, j)$  in spite of  $f(x_t(i, j))$ . It was checked,

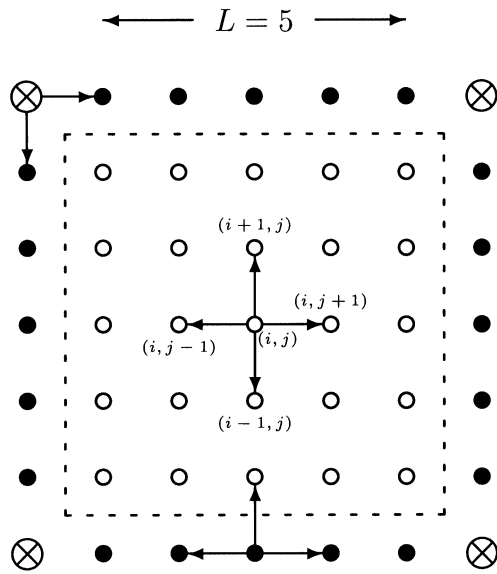


Fig. 1. Sketch of a  $5 \times 5$  CML model of ocean convection, composed by the actual “lattice” (enclosed by the dashed box) and its boundary conditions. Similar symbols are used to denote sites having the same number of coupled neighbors:  $\circ$ ,  $\bullet$  and  $\otimes$  denote coupling to 4, 3 and 2 neighbors, respectively.

whether this makes a difference, and it turned out that the results are qualitatively very similar. Therefore, we kept the diffusion type which is more common in CML studies.

Our CML model of ocean convection consists of a two-dimensional lattice with  $L \times L$  sites coupled to its neighbors, as indicated schematically in Fig. 1. In this paper we work with a  $16 \times 16$  lattice, forming a mesh corresponding to a grid resolution of 250 km over an area of  $4000 \text{ km} \times 4000 \text{ km}$  in the ocean, which is approximately the order of magnitude of the North Atlantic.

As indicated schematically in Fig. 1, the lattice is surrounded by a no-flux boundary where

$$\begin{aligned}
 x_{t+1}^{\text{corner}} &= f(x_t^{\text{corner}}) \\
 &+ \frac{\varepsilon}{4} \left[ \sum_1^2 f(x_t^{\text{neighbor}}) - 2f(x_t^{\text{corner}}) \right] \\
 x_{t+1}^{\text{side}} &= f(x_t^{\text{side}}) + \frac{\varepsilon}{4} \left[ \sum_1^3 f(x_t^{\text{neighbor}}) - 3f(x_t^{\text{side}}) \right].
 \end{aligned}$$

These equations reduce to Eq. (2) when we consider a *forward* scheme discretization [Haltiner & Williams, 1980] for boundary sites perpendicular to the lattice sides.

After a suitable transient, the local value  $x_t$  of the cubic map at each site  $(i, j)$  will have converged to a state near to either the positive or the negative fixed point of the cubic map, namely to either  $x_s^+$  or  $x_s^-$ . As mentioned above, this dichotomy of final states is at the heart of our model: it is used to represent the existence or not of convection at every grid point of the mesh covering the ocean region of interest. Accordingly, we introduce the following convention: positive fixed points  $x_s^+$  correspond to “convective” states while negative fixed points,  $x_s^-$ , correspond to “nonconvective” states. In this way we have effectively codified into our CML model, Eq. (2), the three different local regimes found in the ocean [Lenderink & Haarsma, 1994; Kuhlbrodt et al., 2001].

From the three rectangular boxes in Fig. 2 it is clear that, depending on the value of  $b$ , the CML may be found in any one of the three possible ocean regimes mentioned in the introduction: (i) monostable and nonconvective, (ii) monostable and convective or (iii) bistable. The amplitudes  $x_t(i, j)$  represent the stratification of the ocean at  $(i, j)$ . If this amplitude does not change (fixed point), then  $x_t(i, j) > 0$  corresponds to a lack of stratification (permanent convection — complete vertical mixing) while  $x_t(i, j) < 0$  corresponds to intense stratification (no convection).

As mentioned above, we mimic the convective and nonconvective states of ocean circulation through a cubic local map  $f(x_t(i, j))$  defined in Eq. (1). The parameter  $b$  in Eq. (1) controls the bistability of the map and may be regarded as a sort of buoyancy forcing or, equivalently, as an atmospheric surface temperature.

Ocean stratification has a time-evolution without intrinsic oscillations in the short time scale. Accordingly, we fix  $a = 1.5$  so that the interval of bistability contains only fixed points, as might be seen in the bifurcation diagram shown in Fig. 2. For  $a = 1.5$  one finds bistability to be present in the interval labeled BIS in Fig. 2, delimited by  $-\beta \leq b \leq \beta$ , where  $\beta \equiv \sqrt{6}/18 \simeq 0.136$ , and  $-1.12 \leq x_0 \leq 1.12$ . Inside the BIS box, solid lines indicate the two stable fixed points, the red shading represents the basin of attraction of the positive fixed point,  $x_s^+$ , while the yellow shading indicates the basin of the negative point  $x_s^-$ . The two adjacent boxes NC and C in Fig. 2 indicate the intervals of  $b$  where one finds only a single fixed point, corresponding no-convection ( $x_s^-$ ) or convection ( $x_s^+$ ), respectively.

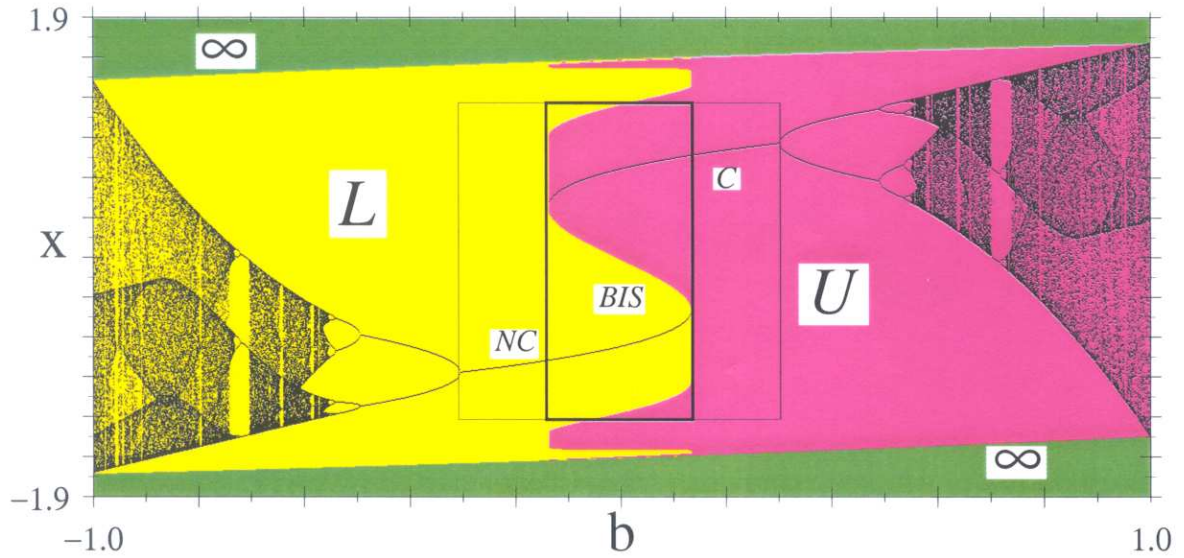


Fig. 2. Bifurcation diagram and corresponding basins of attraction for Eq. (1) with  $a = 1.5$ : the yellow region represents the basin of attraction of attractor  $L$  (“L”ower) and purple indicates the basin of the other attractor  $U$  (“U”pper). The basins are symmetric with respect to the point  $x = 0$  and  $b = 0$ . Inside the box  $-\beta \leq b \leq \beta$ , where  $\beta = \sqrt{6}/18 \simeq 0.136$ , one finds bistability, where each fixed point (solid lines) has a complementary basin of attraction. The basins of  $|\pm\infty|$  are also indicated (green region). NC, BIS and C refer to the nonconvective, bistable and convective intervals of  $b$ , respectively.

From Fig. 2, one sees that for  $b > 0$  the larger region inside the BIS box is covered by the basin of attraction of  $x_s^+$ , while for  $b < 0$  the larger basin is that of  $x_s^-$ . This difference in basin sizes is important for the interpretation of results that follow.

### 3. General Behavior of Convective and Nonconvective States

To probe the dynamical behavior of the model in a general way we perform two independent simulations, each one for a different set of initial conditions (ICs): (i) Gaussian ICs,  $x_0^g$ , given by

$$x_0^g(i, j) = x_s^- + (x_s^+ - x_s^-) \times \exp \left[ - \left( \frac{i - i_c}{2(\Delta i)^2} \right)^2 - \left( \frac{j - j_c}{2(\Delta j)^2} \right)^2 \right], \quad (4)$$

and (ii) “front-like” ICs,  $x_0^f$ , given by

$$x_0^f(i, j) = x_s^- + (x_s^+ - x_s^-) \times \frac{1}{\mathcal{N}} \sum_{k=1}^i \exp \left[ - \left( \frac{k - i_c}{2(\Delta i)^2} \right)^2 \right], \quad (5)$$

$$\mathcal{N} = \sum_{k=1}^L \exp \left[ - \left( \frac{k - i_c}{2(\Delta i)^2} \right)^2 \right], \quad (6)$$

where  $(i_c, j_c)$  is the location of the center of the Gaussian function in (i) and  $i_c$  denotes the location of the front in (ii),  $|x_s^+ - x_s^-|$  is the “amplitude” of the distribution and  $\mathcal{N}$  normalizes the sum in (5). As will become clear in Secs. 4 and 5, these ICs are the most interesting for our purposes. Notice that the numerical values of  $\Delta i$ ,  $\Delta j$  as well as the center of the Gaussian need not be integers, i.e. we may use fronts centered off-lattice, if convenient.

Figure 3 shows the time evolution imposed by Eq. (2) (i.e. in the absence of advection) when started from each set of ICs (4) and (5). As may be seen from these equations, each initial condition assumes a value in  $[x_s^-, x_s^+]$  and belongs to one of the two possible basins of attraction (see Fig. 2). As is clear from Fig. 3, both sets of ICs lead to asymptotic states composed essentially by two nearly constant values, “plateaus”: one localized in the neighborhood of  $x_s^-$  and the other one near  $x_s^+$ .

For Gaussian ICs the upper plateau is delimited by  $(i_c \pm \Delta i, j_c \pm \Delta j)$  while for front-like ICs it is delimited by  $(i_c, i)$  and  $(L, i)$ ,  $1 \leq i \leq L$ . When interchanging  $x_s^- \leftrightarrow x_s^+$  in Eq. (4), i.e. when starting with an inverted Gaussian, we obtain an inverted pattern, “reciprocal” to that seen in Fig. 3. The same is true for front-like ICs. In fact, similar results are also obtained when we replace  $x_s^-$  and  $x_s^+$  by any other fixed values lying in their basins

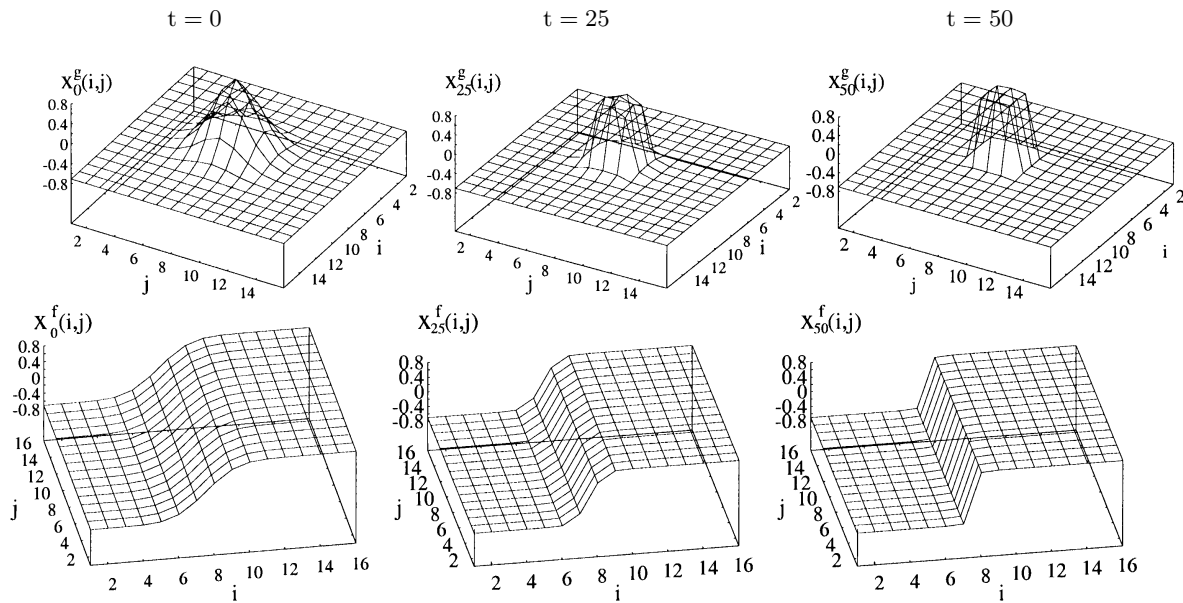


Fig. 3. Time evolution of the lattice for two sets of initial conditions: Gaussian (top row) and front-like (bottom row), both for a diffusion  $\epsilon = 0.075$ . Similar results are obtained for other parameter values. Final states are attained quite fast: the distributions seen for  $t \simeq 50$  are essentially the final states. Here  $b = 0$  and  $\Delta i = \Delta j = 1$ .

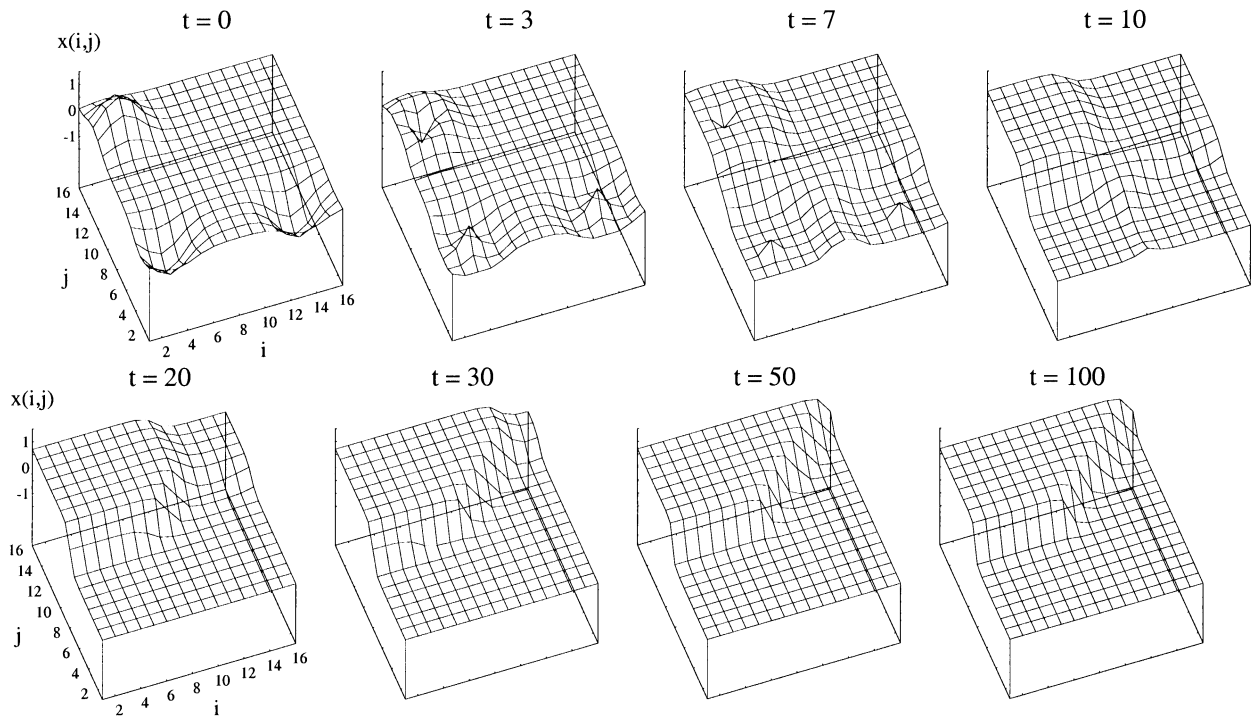


Fig. 4. Plateau configuration reached when starting with a combination of three Gaussian functions. After  $t \simeq 50$  the configuration remains static. As in Fig. 3, here also  $\epsilon = 0.075$ ,  $b = 0$  and  $\Delta i = \Delta j = 1$ . The scales shown are valid for all figures.

of attraction. In particular, when these values are taken to lie in the *same* basin of any one of the fixed points, the lattice evolves to just a single plateau.

Figure 4 illustrates the time-evolution when starting with a combination of three Gaussian functions. As the figure shows, the diffusion leads to a spreading of the Gaussians over the whole lattice, eventually reaching a state (for  $t = 50$ ) in which two plateaus appear, remaining stationary thereafter. This same scenario appears when starting with an arbitrary number of Gaussians. The transient needed to reach the stationary plateaus is quite small (less than about 100 time-steps).

An interesting fact is that the spread induced by the diffusion may temporarily shift the maxima of the Gaussians outside their original basins of attraction. This effect is clearly recognizable by comparing the situations at  $t = 0$  and  $t = 3$  when the two Gaussians with negative maxima move to the basin of the positive fixed point, displaying temporarily positive maxima. Similar behavior is observed when starting with more Gaussians and fronts.

#### 4. Distributions of Convective Cells for the Purely Diffusive Model

In this section we investigate the distribution of convective cells assuming the presence of diffusion only, i.e. assuming the dynamical evolution to be ruled by Eq. (2). First, we study how the number of convective states  $N$  depends on the diffusion  $\varepsilon$  and bistability  $b$ . Second, how  $N$  varies when one allows the bistability to vary along the lattice, i.e. when a gradient of the buoyancy forcing is introduced. Third, how  $N$  varies when bistability varies in hysteresis experiments.

##### 4.1. Diffusion versus bistability

Figure 5 shows the fraction  $R$  of convective states in the lattice,

$$R = \frac{N}{L \times L} = \frac{\text{number of convective states}}{\text{total number of states}}, \quad (7)$$

as a function of  $b$  and  $\varepsilon$  for two sets of ICs, namely, front-like and Gaussian with  $\Delta i = \Delta j = 1.25$ . For Gaussian ICs we impose  $\Delta i = \Delta j$  in order to guarantee the same (radial) symmetry. Both figures show a  $100 \times 100$  discretization of the parameter space and were obtained using transients of

$10^4$  time-steps, although stationarity is frequently obtained after considerably shorter transients. For this reason, the same transient of  $10^4$  time steps was used to obtain all results to be present below.

As is clear from Fig. 5, for both sets of initial conditions there is a marked increase in the number  $N$  of convective states as  $b$  increases, due to the size of the basin of attraction. Furthermore, while for weak diffusion ( $\varepsilon \lesssim 0.1$ ) there is a relatively small increase in  $R$  (smaller for Gaussian than for front-like ICs), when  $\varepsilon \gtrsim 0.1$  it is always possible to define a characteristic value  $b_c$  marking a phase transition so that for  $b > b_c$  there are only convective states on the lattice. Moreover, for  $b < b_c$  and strong diffusion there are only nonconvective states. The value of  $b_c$  depends weakly on  $\varepsilon$  and decreases when one increases the number of initial convective states.

Figure 5(a) was obtained starting with initial conditions given by a positive Gaussian. When starting with a negative Gaussian, one obtains the distribution, shown in Fig. 6, which clearly displays the symmetry

$$R'(\varepsilon, b) = 1 - R(\varepsilon, -b), \quad (8)$$

where  $R'$  refers to the distribution obtained with the negative Gaussian (in Fig. 6) and  $R$  refers to the distribution obtained from a positive Gaussian [Fig. 5(a)].

##### 4.2. Inhomogeneous bistability: Gradient of the buoyancy forcing

In order to mimic the North–South gradient of the buoyancy forcing in the ocean, we now consider the effect of introducing inhomogeneities in the bistability coefficient  $b$ . This is done by starting at  $j = 1$  with  $b = 0$  and increasing it linearly until some value  $b_{\max}$ , at  $j = 16$ , i.e. we introduce a bistability gradient along the  $j$ -axis. Inhomogeneity in the “local” parameters has been shown to be a quite effective mechanism to induce pattern formation in more realistic models [Lind *et al.*, 2001b]. After selecting the bistability, the next task is the choice of suitable initial conditions.

To investigate how a patch of convection develops within a nonconvective environment, we work with the so-called “island” ICs: an island of 12 elements located at the center of our  $16 \times 16$  grid is assumed to be convective while everything else

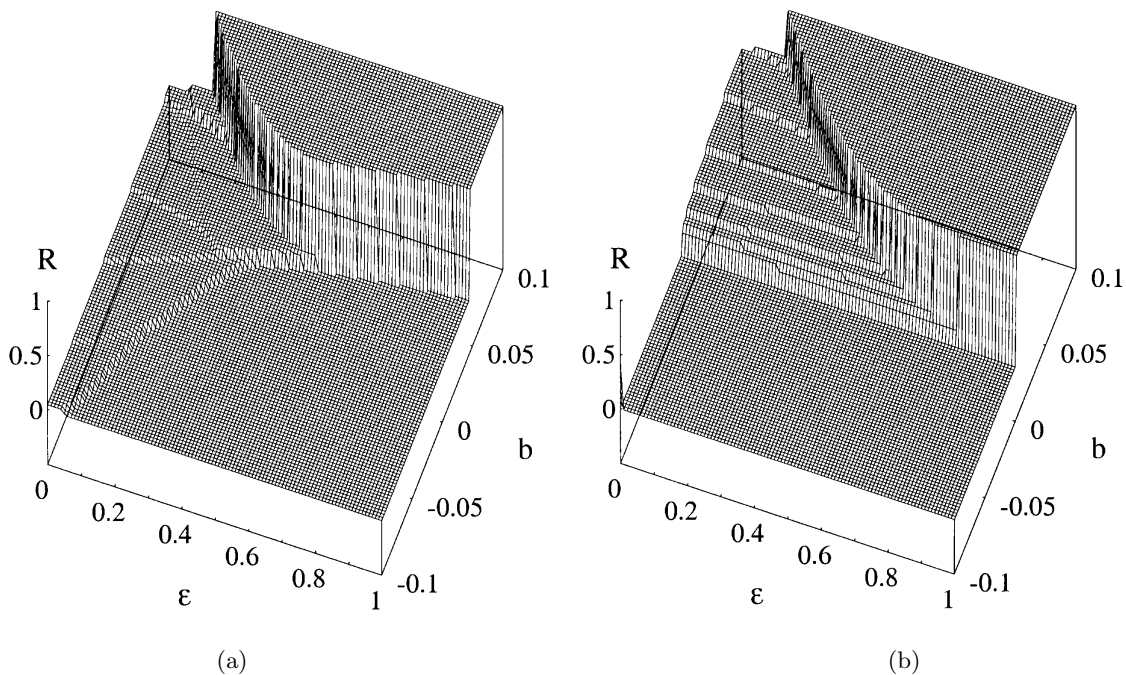


Fig. 5. Fraction  $R$  of convective states as a function of the diffusion and of the bistability for two sets of initial conditions: (a) Gaussian and (b) front-like. Here  $\Delta i = \Delta j = 1.25$ .

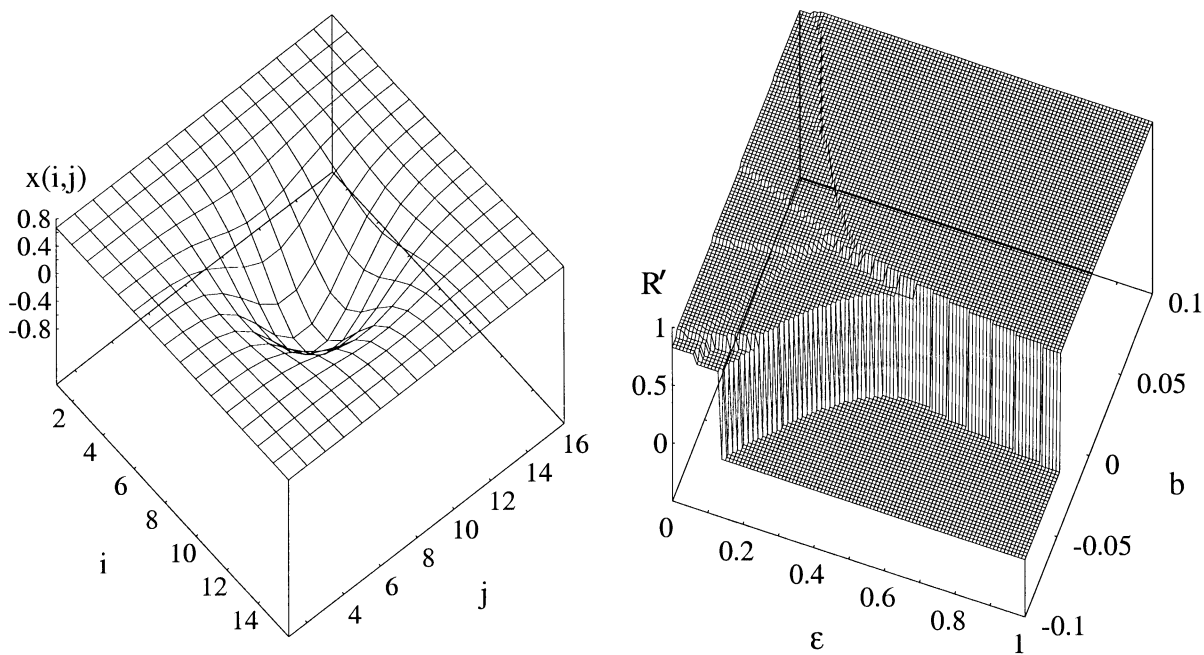


Fig. 6. Distribution of convective states (right) obtained when starting with negative Gaussian ICs (left). This distribution highlights the symmetry defined in Eq. (8) [compare with Fig. 5(a)]. Here  $\Delta i = \Delta j = 1.25$ .

is taken to be nonconvective (see Fig. 7). In other words, the numerical values of  $x_0(i, j)$  for the 12 elements at the center of the lattice are set equal to the positive fixed point of the cubic map while

the remaining values equal the negative fixed point. This starting configuration resembles Gaussian ICs [Eq. (4)] centered off-lattice at  $i_c = j_c = 8.5$  and having  $\Delta i = \Delta j = 1.25$ .

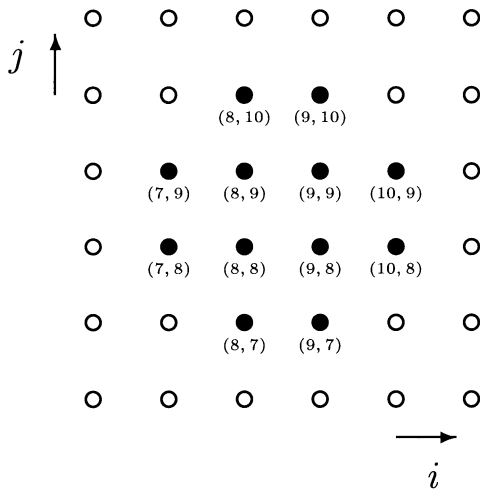


Fig. 7. Sketch of a  $6 \times 6$  sublattice containing an “island” of initial conditions composed by 12 convective states, indicated by black circles, while the remaining symbols denote nonconvective states. Symbols refer to the actual *state* of the site, not to its coordination number as in Fig. 1. The boundary, not shown for simplicity, is the same as before (see Fig. 1).

Figure 8 shows the number of convective elements  $N$  as a function of bistability  $b_{\max}$  and the coupling strength  $\varepsilon$ . When bistability is small, a plateau of  $N = 12$  convective elements is seen for weak diffusion, while the whole grid becomes nonconvective for large diffusion. Figure 8 also shows that for large values of  $b_{\max}$  there is a plateau with 160 convective elements: these are 10 rows of ele-

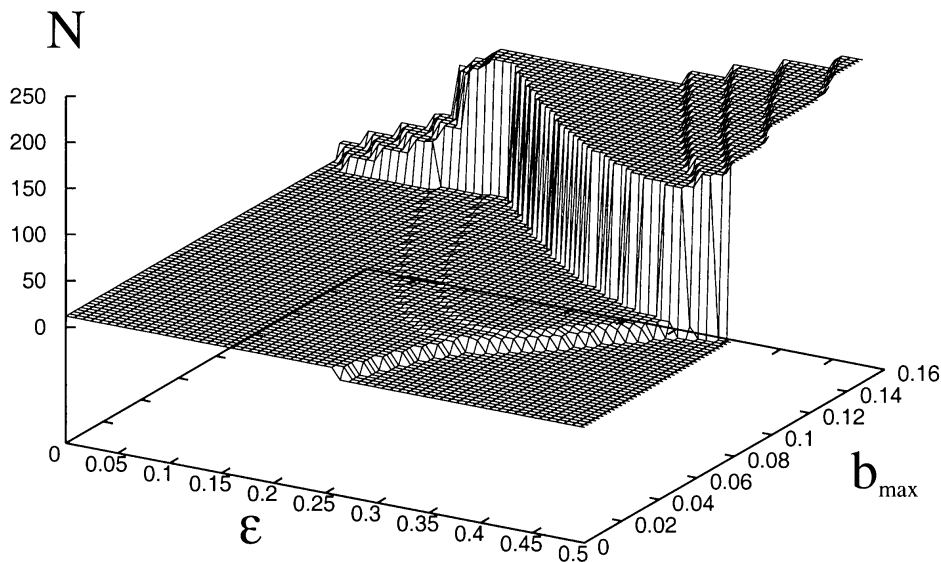


Fig. 8. The number of convective elements as a function of diffusion and  $b_{\max}$ , obtained in the presence of a bistability gradient (see text).

ments, beginning with the lowest  $j$  value of the initial convective island. For large values of  $b_{\max}$  there are convective areas bigger than the ICs, due to the fact that the local cubic maps at large  $j$  values become monostable ( $b > \sqrt{6}/18 \simeq 0.136$ ). For  $b < 0$  the homogeneous nonconvective state appears for smaller values of  $\varepsilon$ . For  $\varepsilon > 0.5$  the distribution resembles that observed in Fig. 5 for  $\Delta i = \Delta j = 1.25$ .

In [Lenderink & Haarsma, 1994] a very similar behavior is found in a three layer ocean model of the North Atlantic. The spreading of convection can be triggered by setting one grid point to be convective in a nonconvective but bistable region of the model Atlantic.

Compared to the physical continuous process, the sharp steps that occur in our results may indicate a biased representation of deep convection [Cessi & Young, 1996]. In the real ocean, there are no “rows” of nonconvective elements that suddenly become convective like in our example, but the transition is a relatively smooth process.

#### 4.3. Sweeping bistability: Hysteresis experiments

In this section we investigate the influence of allowing the bistability coefficient to vary in time. For simplicity, we consider only the time variation of a homogeneous bistability, i.e. at each time step the value of  $b$  is the same in all lattice sites.

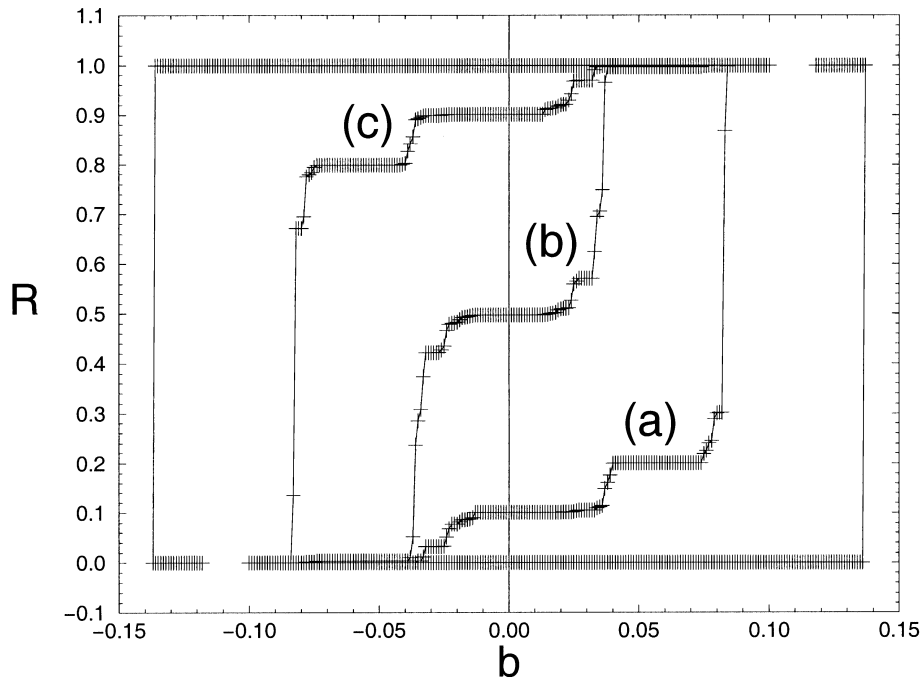


Fig. 9. Hysteresis curves obtained by sweeping  $b$ , after starting from a given initial ratio  $R_0$  of convective cells: (a)  $R_0 = 1/3$ , (b)  $R_0 = 1/2$  and (c)  $R_0 = 2/3$ . Each curve is an average over 400 random initial configurations. Here the diffusion is  $\varepsilon = 0.2$ .

Ocean convection events are triggered by relatively short periods of strong buoyancy forcing (e.g. atmospheric advection of cold air). In our model, the buoyancy forcing is controlled by the parameter  $b$  and, therefore, it is important to investigate its time variation (increase or decrease), namely to check the possible existence of “hysteresis” when  $b$  is changed.

We start with random initial conditions  $x_0(i, j)$  but having a given initial ratio  $R_0$  of convective states. The initial homogeneous value of the bistability is  $b = 0$ . Then, a new value of  $R$  is measured after the system is allowed to evolve until it reaches its attractor. From this value of  $R$  we increase (decrease, in a second hysteresis curve)  $b$ , in steps of 0.001, until the value  $R = 1$  ( $R = 0$ , respectively) is reached. After that,  $b$  is decreased (then increased, respectively) in steps of 0.001. Figure 9 shows the results (hysteresis curves) obtained when starting from three values of  $R_0$ , as indicated, and  $\varepsilon = 0.2$ . Similar curves are obtained for other parameter values.

As the figure shows, starting from  $R_0 = 1/2$  one finds a plateau around  $b = 0.03$  where the increase of  $b$  does not induce any change in  $R$ . There seems to be a critical value of  $b$  where the pattern becomes

again unstable after having reached the plateau. Finally, the entire grid becomes convective ( $R = 1$ ).

Starting with  $R_0 = 1/3$ , one observes that the dynamical evolution acts so as to *reduce*  $R$  during the first transient, because single convective elements do not “survive” in an environment of non-convective elements. Between  $b = 0.04$  and  $b = 0.07$  there is a large plateau where  $R$  does not change at all. The shape of the curves is rather different from the corresponding curve obtained for  $R_0 = 1/2$ .

As seen from Fig. 9, the curves corresponding to  $R_0 = 2/3$  and  $R_0 = 1/3$  are in fact duals of each other due to the symmetry defined by Eq. (8). This remains valid for any pair  $R_0$  and  $R'_0$  that satisfy  $R_0 + R'_0 = 1$ , because of the symmetry of the basin of attraction of the cubic map (see Fig. 2).

The transitions between the plateaus that make the “staircase” shape seen on the hysteresis curves are explained as follows. At certain threshold values of  $b$ , small local patterns (e.g.  $2 \times 2$ ) of non-convecting grid points undergo a transition to the convective state. They switch from one stable fixed point to the other. The threshold values depend on the state of the neighboring elements. They are features of the local neighborhood, and are not finite-size effects of the model. There are no significant

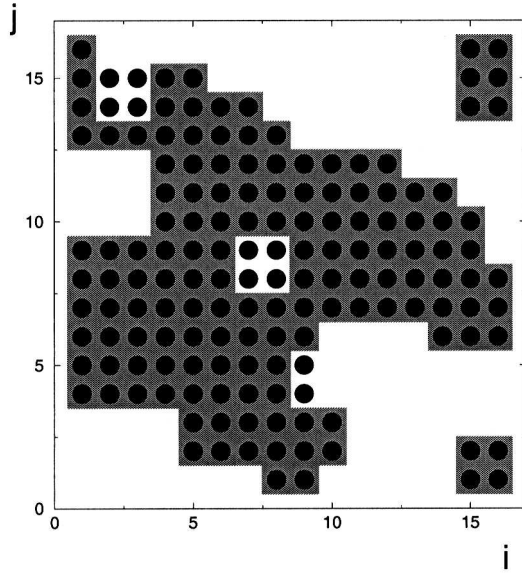


Fig. 10. Transitions of small patterns ( $2 \times 2$ ) to the convective state. White background: nonconvective state. Gray background: convection sets in for  $b = 0.01$ ; black circles: convection sets in for  $b = 0.03$ . Some patterns switch to the convective state for larger bistability  $b$ . This pattern transition is responsible for the staircase behavior seen in Fig. 9.

changes in the hysteresis curves when the lattice size is increased.

The pattern transition is shown in Fig. 10. Local patterns, composed by  $2 \times 2$  sites in the convective or nonconvective state, are stable for  $b = 0.03$ . The plateaus in the hysteresis curves appear since the number of small patterns that become unstable at a certain threshold value is finite and small. We expect the size and shape of small patterns to be different when the coupling of the lattice site is nonlocal [Titz, 2002].

## 5. The Advective CML Model of Ocean Convection

In the ocean, advection is generally stronger than eddy diffusion, a fact indicating that advection related phenomena are of interest in this context.

Recently, advection was introduced [Lind *et al.*, 2002a] and investigated [Lind *et al.*, 2002b] in a rather general CML model for gradient flows by discretizing the advection operator. Such discretization introduces an extra parameter, an “advective velocity”, which acts effectively as an *asymmetry* in the coupling between sites. This extra parameter will be explored in this section.

In two dimensions, the advective velocity is a vector  $\mathbf{v} = (u, v)$ , where  $u$  is the advection in the  $i$  direction and  $v$  the advection in the  $j$  direction. Accordingly, the magnitude and direction of the advection are given by

$$|\mathbf{v}| = \sqrt{u^2 + v^2} \quad \text{and} \quad \theta = \arccos \frac{u}{|\mathbf{v}|}, \quad (9)$$

respectively. A standard discretization of the two-dimensional advection operator (centered differences scheme) yields

$$\begin{aligned} \mathbf{v} \cdot \nabla f \sim & u \frac{f(x_t(i+1, j)) - f(x_t(i-1, j))}{2} \\ & + v \frac{f(x_t(i, j+1)) - f(x_t(i, j-1))}{2}. \end{aligned} \quad (10)$$

Now, following the procedure outlined in [Lind *et al.*, 2002a], we use this expression to extend the purely diffusive model of Eq. (2), obtaining

$$\begin{aligned} x_{t+1}(i, j) = & (1 - \varepsilon)f(x_t(i, j)) \\ & + \frac{\varepsilon - 2u}{4} f(x_t(i+1, j)) \\ & + \frac{\varepsilon + 2u}{4} f(x_t(i-1, j)) \\ & + \frac{\varepsilon - 2v}{4} f(x_t(i, j+1)) \\ & + \frac{\varepsilon + 2v}{4} f(x_t(i, j-1)). \end{aligned} \quad (11)$$

This more general and realistic model, which now includes advection through the parameters  $u$  and  $v$ , corresponds to the discretization of the local time-derivative of a tracer variable  $\chi$ :

$$\frac{\partial \chi}{\partial t} = \Phi_{\text{fluxes}} - \mathbf{v} \cdot \nabla f(\chi). \quad (12)$$

The main effect of advection is to induce the transport of states,  $x_t(i, j)$ , in the direction of  $\mathbf{v}$ . Notice that to guarantee no-flux boundary conditions in the presence of advection one needs to use a forward discretization perpendicularly to the sides of the lattice. For instance, the corner  $(0, 0)$  needs to evolve according to

$$\begin{aligned} x_{t+1} = & f(x_t(0, 0)) \\ & + \frac{\varepsilon}{4} [f(x_t(0, 1)) + f(x_t(1, 0)) - 2f(x_t(0, 0))] \\ & + \frac{u}{2} [f(x_t(1, 0)) - f(x_t(0, 0))] \\ & + \frac{v}{2} [f(x_t(0, 1)) - f(x_t(0, 0))]. \end{aligned} \quad (13)$$

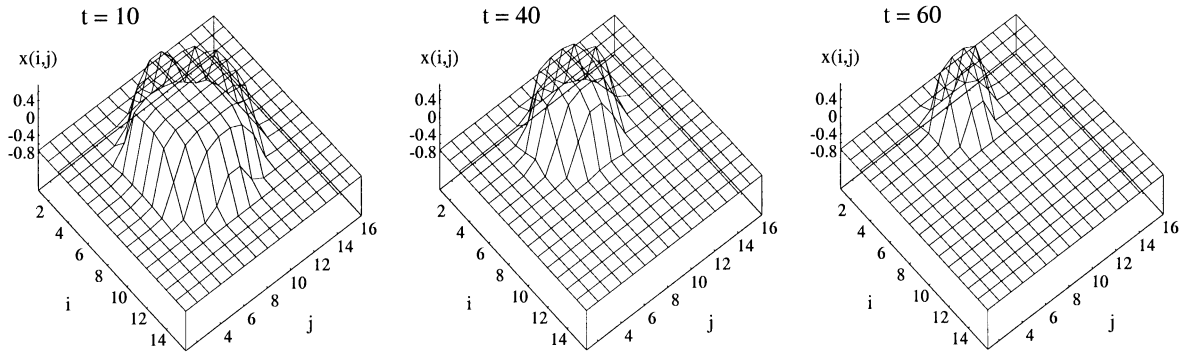


Fig. 11. Deformation and shift induced by the advection on a convective Gaussian island of initial conditions. Here  $\Delta i = \Delta j \sim 1.77$ ,  $b = -0.5$ ,  $\varepsilon = 0.2$  and  $\mathbf{v} = (u, v) = (-0.1, 0)$ .

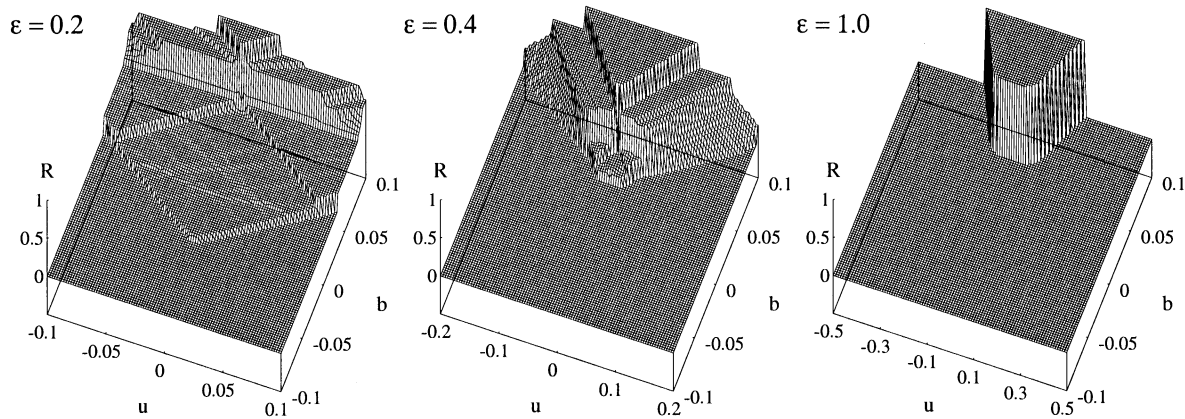


Fig. 12. Distribution of convective states as a function of advection and bistability, when starting with Gaussian initial conditions ( $\Delta i = \Delta j = 1.25$  and  $i_c = j_c = 8.5$ ). The direction of advection is along the  $i$  axis. The ratio  $R$  was determined for 100 values of  $u$  and 100 values of  $b$ , after discarding  $10^4$  time-steps.

Figure 11 illustrates the advection transport for Gaussian ICs, showing that the convective island does not only suffer an obvious net shift, but also a *deformation*. As a consequence, one expects a change in the distributions of convective states. In the following sections, we investigate this change for homogeneous and inhomogeneous bistability.

### 5.1. Homogeneous bistability

Figure 12 shows the dependence of convective-state distribution with  $u$  and  $b$ , for three representative values of the diffusion  $\varepsilon = 0.2, 0.4$  and  $1$ , when starting with Gaussian initial conditions with  $\Delta i = \Delta j = 1.25$  and  $i_c = j_c = 8.5$ . In all cases, the direction  $\theta$  of advection is fixed. As seen from the figure, there is a net change of the critical values beyond which the convective states dominate.

As expected, these distributions are symmetric with respect to  $u$ .

The complicated structure seen for  $\varepsilon = 0.2$  degenerates into a trapezoidal plateau for strong coupling ( $\varepsilon \sim 1$ ). In all situations, higher values of  $b$  tend to favor convective elements.

So far, all results presented were obtained for advectations acting along  $\theta = 0$ . For different values of  $\theta$ , there is a corresponding alignment as shown in Fig. 13.

In general, to have advection means always to have state propagation. Nevertheless, depending on the symmetry of the initial conditions, there is a family of cases for which  $|\mathbf{v}| = -2\varepsilon$ , i.e. the advection cancels the diffusion. The net effect of this cancellation manifests itself in the system as a sort of “instantaneous stationarity” in which the initial

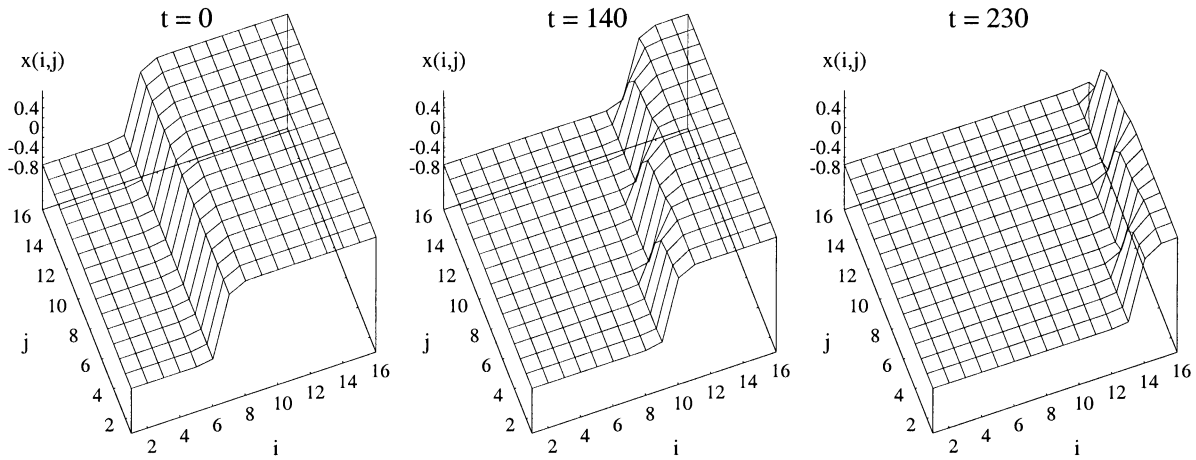


Fig. 13. Asymmetry introduced by an advection acting in a nonperpendicular direction with respect to the initial front. Here  $\Delta i = 1.77$ ,  $i_c = 8.5$ ,  $\varepsilon = 0.2$ ,  $b = 0.05$ ,  $|\mathbf{v}| = 0.0447$  and  $\theta = 45^\circ$ .

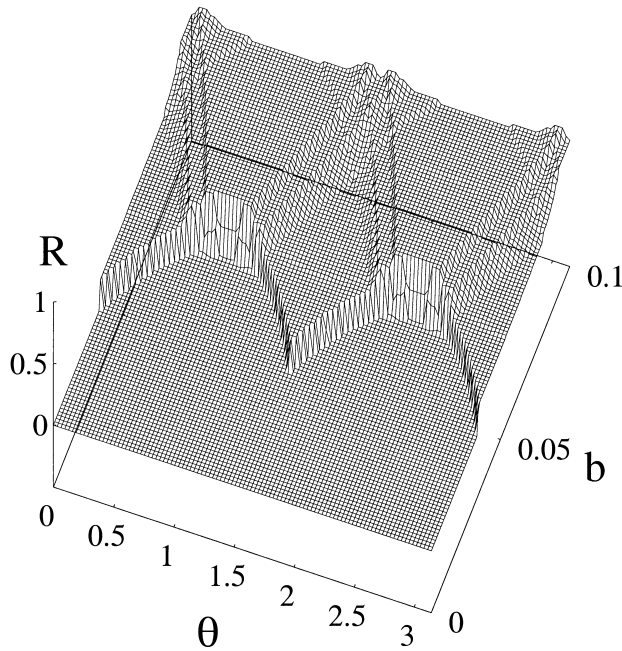


Fig. 14. Distribution of convective states as a function of the bistability  $b$  and  $\theta$  for  $\varepsilon = 0.2$  and  $|\mathbf{v}| = 0.1$ . Note the symmetry with respect to the plane  $\theta = \pi/2$ .

condition already corresponds to the final stationary state. This situation happens mainly for front-like ICs. Such a phenomenon is usually called “pinning fronts” [Kubstrup *et al.*, 1996].

Figure 14 illustrates typical distributions of convective states when the direction  $\theta$  of advection and the bistability  $b$  are varied. The distribution is symmetric with respect to  $\theta = \pi/2$ , when the advection has a direction perpendicular to the  $i$

direction. As seen from the figure, the appearance of convective states is favored for  $\theta = k\pi/2$ , where  $k = 0, 1, 2, \dots$ .

Random ICs are useful to assess the general behavior of convection states in the ocean where many different initial conditions can occur. Figure 15 shows distributions of convective states obtained using random IC configurations, where the IC of the local element is either the convective or the nonconvective fixed point of the uncoupled map. The distributions shown are averages of the  $R$  values obtained by sampling 100 initial configurations. The bistability is set as  $b = 0.1$  to favor local convective states. As seen in Fig. 15(a), the pattern formation depends in a very complicated way on the direction of advection. For different diffusion levels one finds completely different angles characterizing the maximal number of convective elements. The same characterization holds for the dependence on  $\theta$  and  $|\mathbf{v}|$  [see Fig. 15(b)].

These results seem to indicate that, depending on the advective direction  $\theta$ , the spreading behavior of convection might be systematically biased in the square-grid representation of ocean models. One could argue that the boundary of the lattice will introduce anisotropic effects. This can be checked with lattices having a more or less circular boundary. In this way, we observed that there are no significant differences between square or circular lattices. Accordingly, we conclude that the square-grid bias found here only depends on the grid geometry and not on the shape of the boundary.

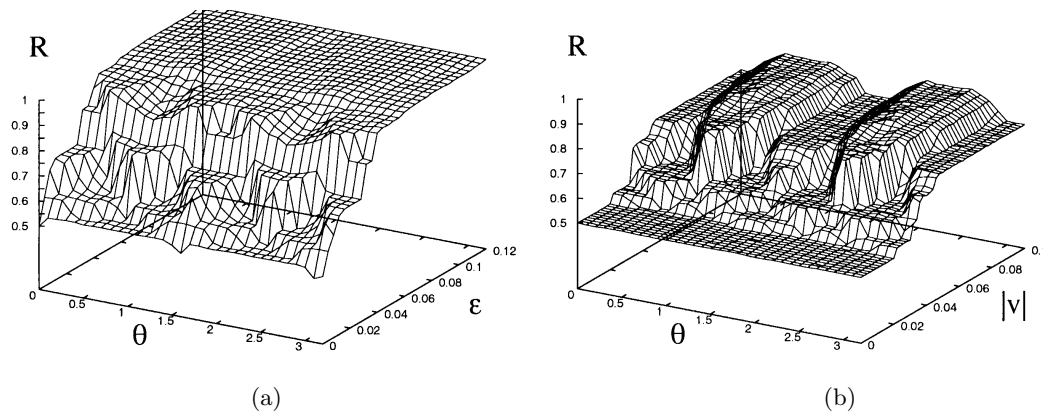


Fig. 15. Distribution of convective states for homogeneous bistability,  $b = 0.1$ , as a function of (a)  $\theta$  and  $\epsilon$  with  $|\mathbf{v}| = 0.05$ ; (b)  $\theta$  and  $|\mathbf{v}|$  with  $\epsilon = 0.024$ . Random initial conditions were used in both cases.

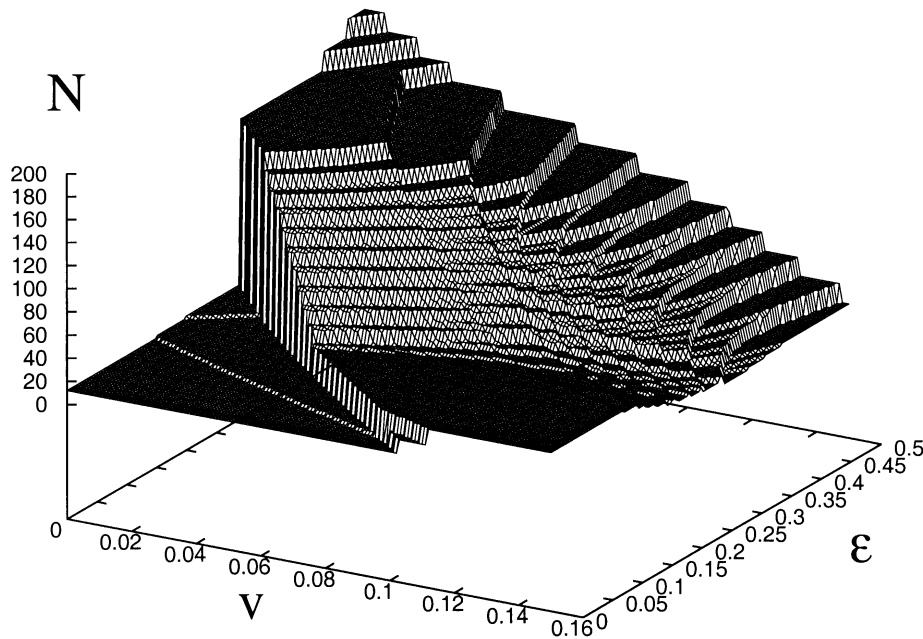


Fig. 16. The number of convective states as a function of diffusion and advection for inhomogeneous bistability. Here  $b_{\max} = 0.1$ ,  $\theta = \pi/2$  and island ICs. Weak advection induces convection while strong advection destroys it.

### 5.2. Inhomogeneous bistability

We now investigate the effect of more realistic situations in which there is an inhomogeneous bistability  $b$ , attempting to mimic an oceanographic scenario for deep ocean convection. To this end we use island ICs subjected to an advection acting along the  $j$  direction. As before, the bistability increases linearly along the  $j$  direction.

Figure 16 shows that the role of advection is two-fold: weak advection induces the creation of convective areas while strong advection destroys it.

The role of diffusion is nontrivial: increasing diffusion yields increasing convection but at higher levels diffusion can also destroy convective areas.

At low diffusion and advection levels, the island ICs give in fact the final configuration of the lattice. Increasing diffusion yields a jump towards the same plateau as in Fig. 8, containing 160 convective elements. On the other hand, increasing advection, stair steps of 16 elements occur. The advection pushes the border of the convective area towards larger  $j$  levels. This behavior is illustrated

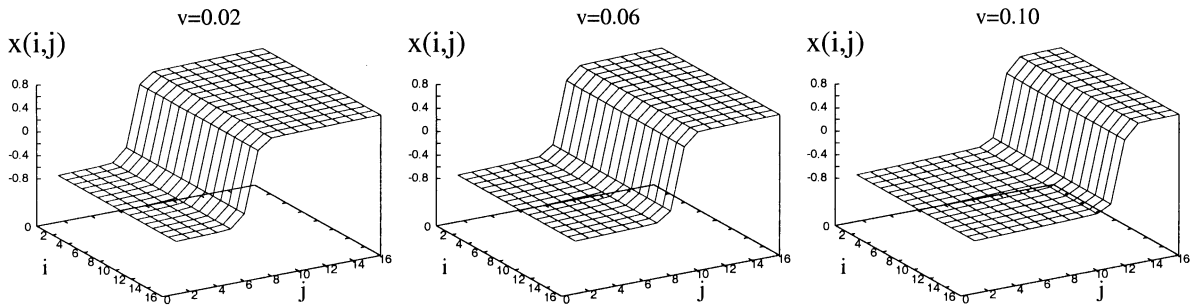


Fig. 17. An increase in the advection  $v$  shifts the convective area to higher  $j$  levels. In all three cases the fronts shown do not vary in time. Here  $\varepsilon = 0.4$ ,  $b_{\max} = 0.1$ .

in Fig. 17 for three values of  $v$ . For large advection and very weak diffusion, the convective patch spreads towards maximal  $j$  levels but does not broaden in the direction of  $j$ .

## 6. Conclusions and Outlook

The purpose of this paper is to introduce a novel CML approach for investigating discretization effects in ocean models due to the presence of convection. The interaction of local nonlinear dynamics with global parameters in ocean models is studied in order to clarify the effects of convection parameterization. This parameterization is commonly done by convective adjustment and can exhibit local bistability and cause problems arising from discretization. We have demonstrated that coupled map lattices are convenient tools to model the interplay between global effects, like diffusion and advection, and local nonlinear dynamics. In the present CML, each of these effects is controlled by a single parameter: the diffusion constant, the velocity and a parameter that controls bistability and corresponds to buoyancy forcing.

First, we neglect advection to isolate the effects of diffusive coupling alone. For given initial conditions and large values of the diffusion constant the final steady state is characterized by a phase transition to a homogeneous state. Buoyancy forcing determines whether the entire lattice becomes convective or nonconvective. For small values of the diffusion constant the final state remains close to the chosen initial conditions.

The most important effect appears in hysteresis experiments with randomly distributed initial conditions in which buoyancy forcing is temporarily increased. We observe that the total number of

convective elements in the lattice increases with the buoyancy forcing — but in steps rather than continuously. This effect persists even when we average over a large ensemble of simulations. Such staircase behavior is caused by local patterns that become unstable for certain thresholds of buoyancy forcing. We suspect that similar behavior can be found in 3D ocean models, introducing spurious abrupt changes in spreading of convection.

Second, since advection plays a crucial role in ocean dynamics, we also consider the interplay between advection and diffusion. For small values of the advective velocity and strong buoyancy forcing, the area of convective activity expands only if the diffusion constant is sufficiently large. Otherwise, it will shrink and disappear. This result is physically intuitive and lends credibility to the CML ansatz.

For large values of the advective velocity the final state depends in a complicated way on the direction of the velocity vector. The main difference is observed between a velocity vector along lattice axes and one at an angle of  $45^\circ$ . Whether the direction of the velocity vector favors or opposes the spreading of convection depends both on the diffusion constant and on the magnitude of the velocity. Again, these results remain valid for the average over an ensemble of simulations with initial conditions randomly distributed in space. This dependence on the direction of the velocity might as well appear in 3D ocean models and thus bias the spreading behavior of convection. As a matter of fact, preliminary numerical experiments indicate that with a hexagonal grid the results are much more isotropic than those found with a rectangular grid. Hexagonal grids are already being used in a weather forecast model [Workshop, 2000].

In addition to the influence of the velocity direction, our results point also at the importance

of its magnitude. Intermediate velocity levels favor spreading of convection while very small or large magnitudes tend to suppress it.

Finally, we would like to mention that we have also employed a more realistic two-layer ocean model in which the temperature and the salt content are the model variables. The convection process depends then on the density difference between the two layers. The results obtained with this more elaborate model are very similar to those reported here. In particular, we found again artificial hysteresis steps and sensitivity to the direction of advection, which do not depend on the lattice size. This corroborates our suspicion that these effects occur in 3D ocean models as well. A detailed work with this more realistic model, emphasizing oceanographic purposes, is under way and will be published elsewhere.

All in all, our results stress the need for improving deep convection parameterization, with the aim of suppressing local discretization effects. This conclusion is in line with an earlier study of Cessi and Young [1996], which used a different modeling approach. They already suggested to include the strong lateral mixing caused by convection events as a remedy to the spurious discretization effects. In addition to that, our results clearly stress the relevance of an appropriate choice of grid geometry for ocean models. We suspect that a grid geometry with hexagonal cells leads to a better representation of convective processes than a geometry with rectangular cells. A detailed comparison concerning the influence of larger neighborhoods in the CML needs now to be done. It would also be of interest to investigate the impact of basin asymmetries on the local bistability, using, for instance, a quartic map [Jánosi & Gallas, 1999].

## Acknowledgments

The authors would like to thank Prof. S. Rahmstorf, Universität Potsdam and Potsdam-Institut für Klimafolgenforschung, for useful discussions. This work is part of a German–Portuguese (DAAD-GRICES) and Brazilian–Portuguese (CAPES-GRICES) bilateral cooperations. P. G. Lind thanks *Fundação para a Ciência e a Tecnologia*, Portugal, for a doctoral fellowship. J. A. C. Gallas is a CNPq Research Fellow, Brazil. S. Titz, T. Kuhlbrodt, J. Kurths and U. Feudel were supported by the DAAD and the Deutsche Forschungsgemeinschaft (Sfb 555).

## References

- Beck, C. [1995] “Chaotic quantization of field theories,” *Nonlinearity* **8**, 423–441.
- Brunnet, L. G. & Gallas, J. A. C. [1998] “Exploring collective behaviors with a multi-attractor quartic map,” *Physica* **A257**, 329–333.
- Cabral, F. Lago, A. & Gallas, J. A. C. [1993] “A picture book of two families of cubic maps,” *Int. J. Mod. Phys.* **C4**, 553–568.
- Cessi, P. [1996] “Grid-scale instability of convective-adjustment schemes,” *J. Marine Res.* **54**, 407–420.
- Cessi, P. & Young, W. R. [1996] “Some unexpected consequences of the interaction between convective adjustment and horizontal diffusion,” *Physica* **D98**, 287–300.
- Haltiner, G. J. & Williams, R. T. [1980] *Numerical Prediction and Dynamic Meteorology* (John Wiley).
- Hecht, M. W., Wingate, B. A. & Kassis, P. [2000] “A better, more discriminating test problem for ocean tracer transport,” *Ocean Modelling* **2**, 1–15.
- Heidvogel, D. B. & Beckmann, A. [1998] *Numerical Ocean Circulation Modeling*, Series on Environmental Science and Management (World Scientific, Singapore).
- Hilgers, A. & Beck, C. [2001] “Higher-order correlations of Tchebyscheff maps,” *Physica* **D156**, 1–18.
- Jánosi, I. M. & Gallas, J. A. C. [1999] “Globally coupled multiattractor maps: mean field dynamics controlled by the number of elements,” *Phys. Rev.* **E59**, R28–R31.
- Kaneko, K. [1993] *Theory and Applications of Coupled Map Lattices* (John Wiley, NY).
- Kaneko, K. & Tsuda, I. [2000] *Chaos and Beyond* (Springer-Verlag, Berlin).
- Kapral, R. & Oppo, G.-L. [1986] “Competition between stable states in spatially-distributed systems,” *Physica* **D23**, 455–463.
- Kubstrup, C., Herrero, H. & Pérez-García, C. [1996] “Fronts between hexagons and squares in a generalized Swift–Hohenberg equation,” *Phys. Rev.* **E54**, 1560–1569.
- Kuhlbrodt, T., Titz, S., Feudel, U. & Rahmstorf, S. [2001] “A simple model of seasonal open ocean convection, Part II: Labrador Sea stability and stochastic forcing,” *Ocean Dyn.* **52**, 36–49.
- Lenderink, G. & Haarsma, R. J. [1994] “Variability and multiple equilibria of the thermohaline circulation associated with deep-water formation,” *J. Phys. Oceanogr.* **24**, 1480–1493.
- Lind, P. G., Corte-Real, J. A. & Gallas, J. A. C. [2001a] “The distribution of periodic and aperiodic pattern evolutions in rings of diffusively coupled maps,” *Int. J. Bifurcation and Chaos* **11**, 2647–2661.
- Lind, P. G., Corte-Real, J. A. & Gallas, J. A. C. [2001b] “Traveling waves induced by parameter fluctuations in rings of coupled maps,” *Physica* **A295**, 297–300.

- Lind, P. G., Corte-Real, J. A. & Gallas, J. A. C. [2002a] "Using advection to control the velocity of patterns in rings of maps," *Physica* **D168–D169**, 93–105.
- Lind, P. G., Corte-Real, J. A. & Gallas, J. A. C. [2002b] "Modeling velocity in gradient flows with coupled-map lattices with advection," *Phys. Rev.* **E66**, 016219.
- Molemaker, M. J. & Dijkstra, H. [2000] "Stability of a cold core eddy in the presence of convection: Hydrostatic versus nonhydrostatic modeling," *J. Phys. Oceanogr.* **30**, 475–494.
- Peixoto, J. P. & Oort, A. H. [1992] *Physics of Climate* (American Institute of Physics, NY).
- Pikovsky, A. S. & Kurths, J. [1994] "Do globally coupled maps really violate the law of large numbers?" *Phys. Rev. Lett.* **72**, 1644–1647.
- Rahmstorf, S. [1995] "Bifurcations of the Atlantic thermohaline circulation in response to changes in the hydrological cycle," *Nature* **378**, 145–149.
- Rahmstorf, S. [2001] "A simple model of seasonal open ocean convection Part I: Theory," *Ocean Dyn.* **52**, 26–35.
- Titz, S. [2002] *Bifurcations of Oceanic Overturning and Convection in Conceptual Models of the Thermohaline Circulation*, PhD thesis, Mathematisch-Naturwissenschaftliche Fakultät der Universität Potsdam, Germany, January.
- Vellinga, M. [1998] "Multiple equilibria in ocean models as a side effect of convective adjustment," *J. Phys. Oceanogr.* **28**, 621–633.
- Welander, P. [1982] "A simple heat salt oscillator," *Dyn. Atmos. Oceans* **6**, 233–242.
- Workshop [2000] *Workshop on Developments in Numerical Methods for Very High Resolution Global Models*, European Centre for Medium-Range Weather Forecasts, ECMWF, Workshop Proc., Vol. 59.